

We are IntechOpen, the world's leading publisher of Open Access books Built by scientists, for scientists

6,900

Open access books available

186,000

International authors and editors

200M

Downloads

Our authors are among the

154

Countries delivered to

TOP 1%

most cited scientists

12.2%

Contributors from top 500 universities



WEB OF SCIENCE™

Selection of our books indexed in the Book Citation Index
in Web of Science™ Core Collection (BKCI)

Interested in publishing with us?
Contact book.department@intechopen.com

Numbers displayed above are based on latest data collected.
For more information visit www.intechopen.com



Fluorescence Cross-Correlation Spectroscopy for Real-Time Monitoring of Exogenous DNA Behavior in Living Cells

Akira Sasaki and Masataka Kinjo

*Graduate School of Advanced Life Science, Hokkaido University
Japan*

1. Introduction

Many kind of DNA transfection techniques have been developed and widely used in the field of biochemical assay (Boussif et al., 1995, Chu et al., 1987, Felgner et al., 1987). Since recent development of fluorescent proteins such as green fluorescent protein (GFP), its variants and bio sensors, DNA transfection techniques play a greater role in the field of cell biology especially in bioimaging studies. DNA transfection is also used as a key technology to gene therapy (Selkirk, 2004, Schaffert et al., 2008). Thus the development of gene delivery vector with high efficiency is expected. Gene delivery systems with artificial nonviral vectors are widely used in the research field of cell biology and also in the clinical field as gene therapy to promote exogenous gene expression or inhibit production of a target protein. Nonviral vectors have advantages such as a low immune response and no risk of a disorder, which might be caused by native viral vector genome integration (Thomas et al., 2003). However, nonviral vectors need to overcome the disadvantage of low gene expression efficiency compared with native viral vectors (Luo et al., 2000). To increase the expression efficiency, it is needed to know gene delivery mechanisms. In general, complexes of exogenous DNAs and a cationic polymer or cationic lipid, commonly used as nonviral vectors, are internalized to target cells by endocytosis. Then a sequential process progresses spontaneously with escape from endosomes, dissociation of complexes, and diffusion of naked DNAs in the cytoplasm to the nucleus (Fig. 1) (Elouahabi et al., 2005).

However, such dynamic properties of transfected DNAs are not yet clearly distinguished because of the lack of suitable technique to observe intracellular DNA behavior. Fluorescence correlation spectroscopy (FCS) is a method based on observation of fluorescence intensity fluctuations that is the result of single fluorescent molecules diffuse in and out of small detection area (Fig. 2A, B) (Eigen et al., 1994). FCS technique can be applied for quantification of the absolute number of fluorescently labeled particles and measuring the molecular weight or size with extremely high sensitivity in a small sample volume, and a physical separation procedure is not needed. Therefore, FCS has currently employed to investigate molecular size or interactions *in vitro* and *in vivo* (Kinjo et al., 1995, Kitamura et al., 2006, Remaut et al., 2007, Kinjo et al., 2010). Dual color fluorescence cross-correlation spectroscopy (FCCS), an extended technique of FCS, can monitor molecular interactions directly in addition to parameters given from FCS measurements (Saito et al., 2004, Kogure et al., 2006, Bacia et al., 2007, Kim et al., 2007).

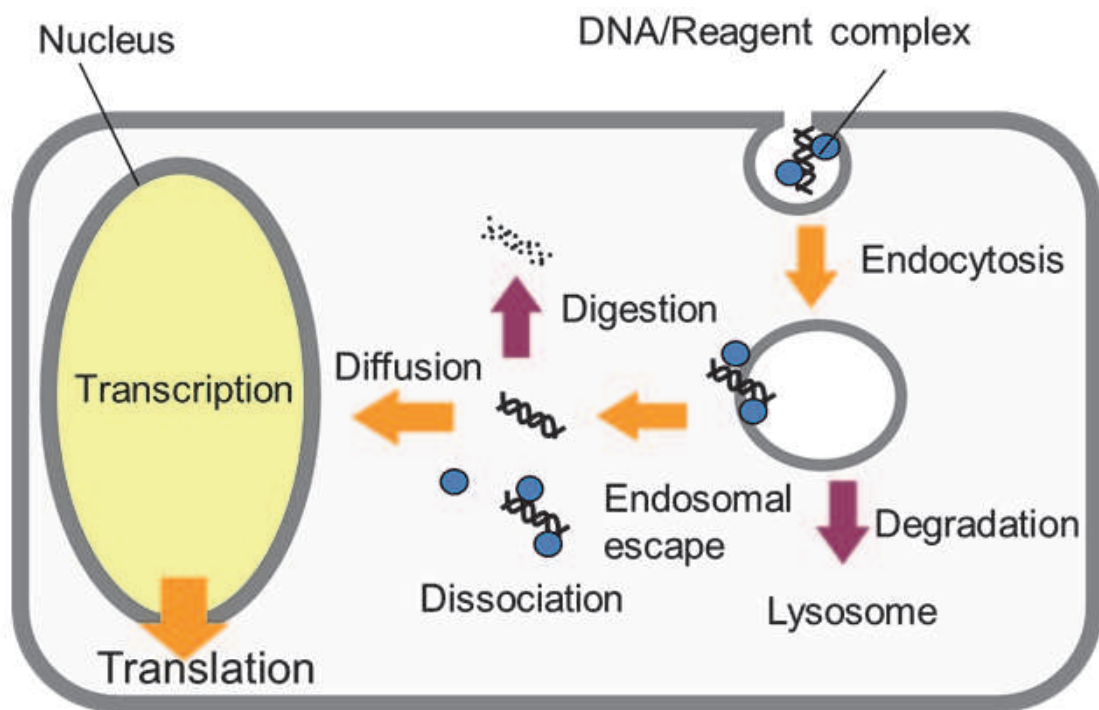


Fig. 1. Schematic diagram of intracellular gene delivery pathway.

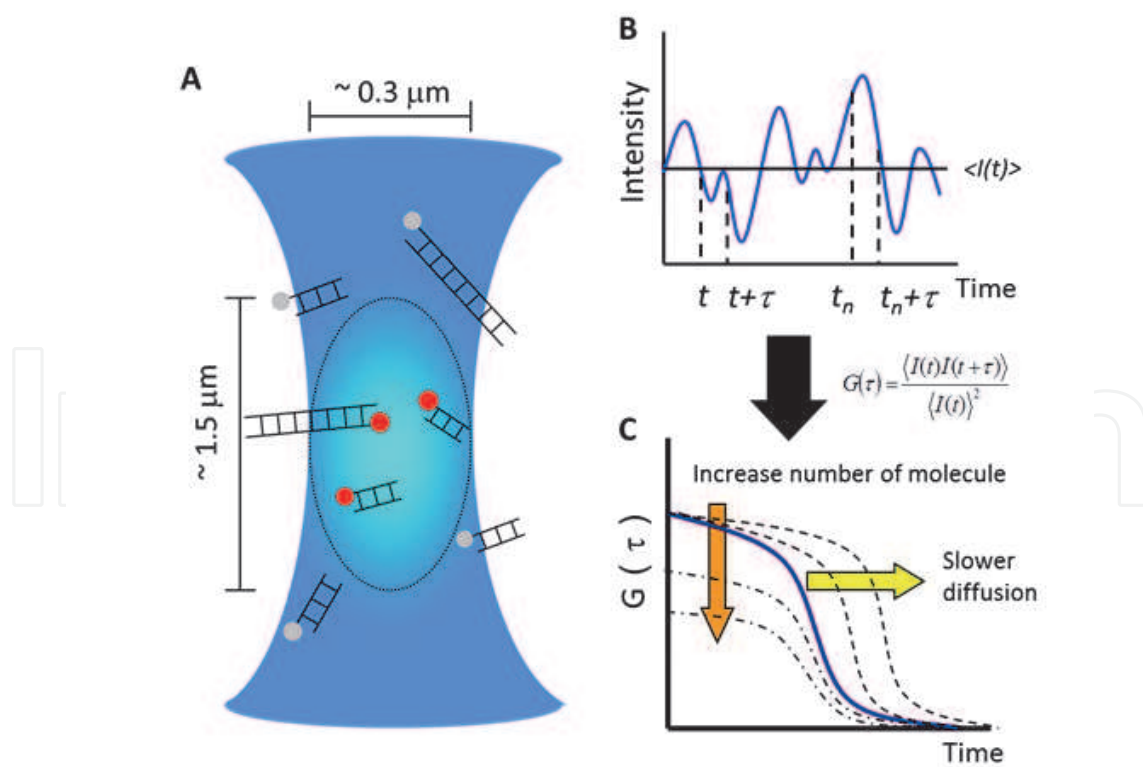


Fig. 2. Schematic diagram of FCS. (A) Schematic of observation area of FCS (confocal volume). (B) Obtained fluctuation of fluorescence intensity. (C) Autocorrelation functions (ACFs).

When the two target molecules are interacting, they will move together through the observation area and have synchronized fluorescence fluctuations in both two channels (Fig. 3A). On the other hand, the fluctuations are not correlated when these molecules move independently of one another (Fig. 3B). In this chapter, We describe the advantages of FCCS technique for the research field of gene therapy. In our research, FCCS technique was applied to study i) the behavior of exogenous DNA in living cells (Sasaki et al., 2010) and ii) the formation of DNA/carrier complex. In these cases, FCCS revealed the DNA degradation by nucleases and DNA-cationic polymer interactions to form DNA/carrier complex in real-time.

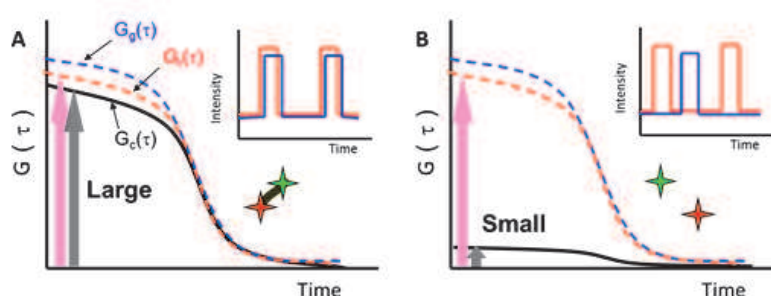


Fig. 3. Schematic diagram of FCCS. Auto and Cross-correlation functions (CCFs) of two fluorescent probes are connected (A) or separated (B).

2. Analysis of fluorescence cross-correlation spectroscopy

The FCCS setup consists of excitation, detection, and data processing systems similar to that of a typical laser-scanning confocal fluorescence microscope with high numerical-aperture (NA) objective.

Laser beams are focused on the coverslip via a confocal optic system to subfemto-liter size of observation area is generated. Emitted fluorescence signal is detected two avalanche photodiode (APD) through dichroic mirror (DM) and filter sets (barrier filter; BF) for each color channels (Fig. 4).

The FCS data are interpreted in terms of autocorrelation functions ($G(\tau)$) (Fig. 2C), that give information on the diffusion time (DT) and the number of molecules (N) in observation area. Diffusion constant can be estimated from DT and size of observation area (Eigen et al., 1994).

The fluorescence autocorrelation functions of the red and green channels, $G_r(\tau)$ and $G_g(\tau)$, and the fluorescence cross-correlation function, $G_c(\tau)$, are calculated by

$$G_x(\tau) = \frac{\langle I_i(t) \cdot I_j(t + \tau) \rangle}{\langle I_i(t) \rangle \langle I_j(t) \rangle} \quad (1)$$

where τ denotes the time delay. I_i is the fluorescence intensity of the red channel ($i = r$) or green channel ($i = g$), $G_r(\tau)$ and $G_g(\tau)$ denote the autocorrelation functions of red ($i = j = x = r$), and green ($i = j = x = g$) respectively, or $G_c(\tau)$ denotes cross-correlation function ($i = r, j = g$, and $x = c$). Acquired $G(\tau)$ were generally fitted by a one- ($i = 1$) or two-component model ($i = 2$) as

$$G(\tau) = 1 + \frac{1-f + f \exp(-\tau/\tau_i)}{N(1-f)} \sum_i F_i \left(1 + \frac{\tau}{\tau_i}\right)^{-1} \left(1 + \frac{\tau}{s^2 \tau_i}\right)^{-1/2} \quad (2)$$

where F_i and τ_i are the fraction and diffusion time of component i , respectively. N is the average number of fluorescent particles in the observation area defined by radius ω and length $2z$, and s is the structural parameter representing the ratio $s = z/\omega$. The diffusion time (τ_i) corresponds to the average time for diffusion of fluorescent particles across the detection area, which reflects the size of particles. f is the average fraction of triplet state molecules and τ_i is triplet relaxation time (Widengren et al., 1995, Rigler et al., 1993). The distribution histogram of diffusion times was constructed using the CONTIN algorithm (Provencher, 1982, Björling et al., 1998).

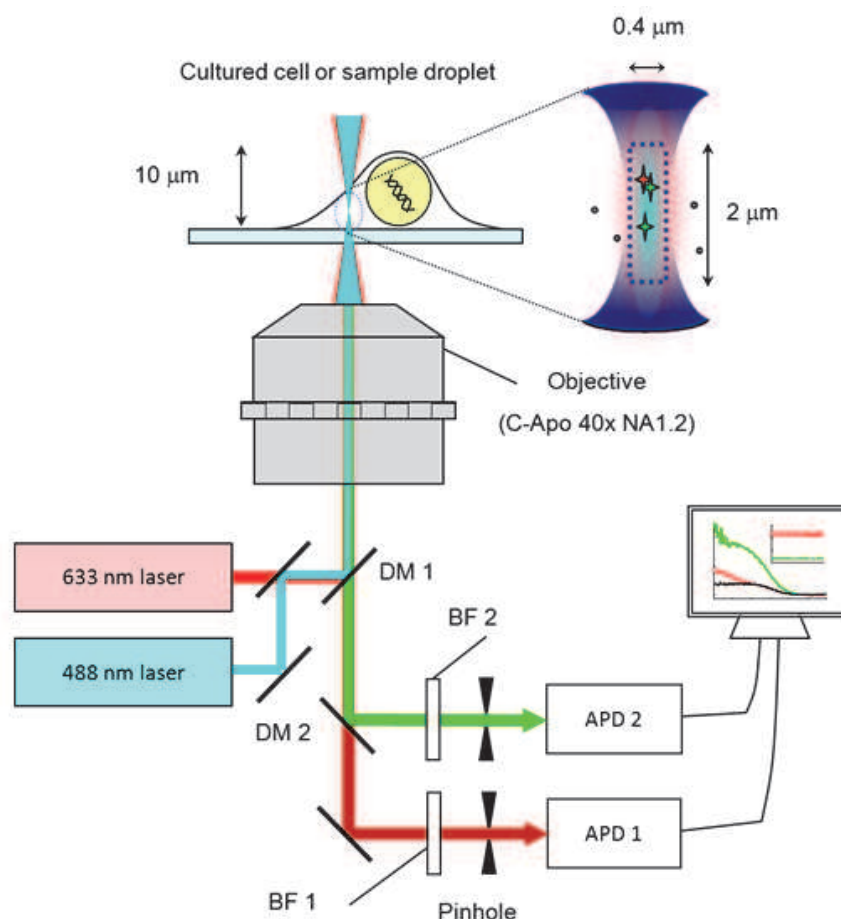


Fig. 4. Experimental setup for FCS and FCCS.

Instead of evaluating discrete diffusion processes with distinct species and their characteristic diffusion times, the dynamic motion of DNAs in the cell can be distributed with regard to their diffusion times using the distribution function $P(\tau D_i)$. The average numbers of red fluorescent particles (N_r), green fluorescent particles (N_g), and particles that have both red and green fluorescence (N_c) can be calculated by

$$N_r = \frac{1}{G_r(0) - 1}, \quad N_g = \frac{1}{G_g(0) - 1} \quad (3)$$

$$N_c = \frac{G_c(0) - 1}{[G_r(0) - 1] \cdot [G_g(0) - 1]} \quad (4)$$

respectively. When N_r and N_g are constant, $(G_c(0)-1)$ is directly proportional to N_c . For quantitative evaluation of cross-correlations among various samples, the cross-correlation amplitude is normalized by autocorrelation amplitude (relative cross-correlation amplitude; RCA). RCA can be calculated by

$$RCA_g = \frac{G_c(0) - 1}{G_g(0) - 1} \quad (5)$$

$$RCA_r = \frac{G_c(0) - 1}{G_r(0) - 1} \quad (6)$$

respectively. The ratio of interacted molecule in red or green molecules can be obtained from equations 3 and 4 as

$$\frac{G_c(0) - 1}{G_g(0) - 1} = \frac{N_c}{N_r} \quad (7)$$

$$\frac{G_c(0) - 1}{G_r(0) - 1} = \frac{N_c}{N_g} \quad (8)$$

respectively. RCA_g shows the ratio of interacted molecules in the red molecules (N_c/N_r) (Eqs. 5 and 7) and RCA_r shows the ratio of interacted molecules in the green molecules (N_c/N_g) (Eqs. 6 and 8). FCCS measurement also gives the parameter of photon counts per molecule (CPM) of each fluorescent species. CPM is represented by count rate divided by number of particles.

3. Monitoring exogenous DNA degradation in living cells

Physical approaches such as microinjection (Zhang et al., 2008) and electroporation (Somari et al., 2000) are performed to incorporate naked DNAs directly into cytoplasm and/or nucleus across the plasma membrane. On the other hand, DNAs are released into cytoplasm as naked shape and then the DNAs diffuse in the cytoplasm to the nucleus in the case of using gene carrier. The diffusion of exogenous DNAs in cytoplasm is relatively slow compared with that in solution (Dauty et al., 2005), and it is hard that large DNA goes cross the nuclear membrane in short time. Under such conditions in cytoplasm, the existence of nuclease degradation in cytoplasm is suggested (Pollard et al., 2001, Lechardeur et al., 1999, Fisher et al., 1993). It is presumed that the translocation and nuclear uptake of transfected DNA compete with digestion. Therefore, it is important to investigate behavior of naked exogenous DNAs in cytoplasm to achieve efficient gene delivery and expression. The cytoplasmic degradation for exogenous DNAs can work as a barrier against efficient gene delivery. However, little is known about the degradation mechanism because it is difficult to characterize the degradation process of exogenous DNA in living cells. The purpose of this section was to investigate the mechanism of exogenous DNA degradation in situ, in cytoplasm, by analyses of diffusion properties of DNAs and to determine the effects of cytoplasmic degradation on the gene

expression rate. Thus we employed FCS to measure the diffusion properties of DNAs, and FCCS to monitor the degradation of DNAs by cytoplasmic nucleases at the single molecule level. Furthermore, we predicted that exonucleases would work as the main barrier in cytoplasm, so a capped or redundant structure was attached to the transfected DNA to enhance the expression of the protein EGFP.

3.1 Diffusion analysis of constructed DNAs in solution

A series of linear DNAs from 23 bp to 500 bp that were labeled with rhodamine green (RG) and Cy5 on both 5' ends (RG-DNA-Cy5) were synthesized by PCR. Autocorrelation curves of the green fluorescence channel ($G_g(\tau)$) and red fluorescence channel ($G_r(\tau)$), and a cross-correlation curve ($G_c(\tau)$) were obtained by FCCS measurements of RG-DNA-Cy5 in solution (Fig. 5A-D).

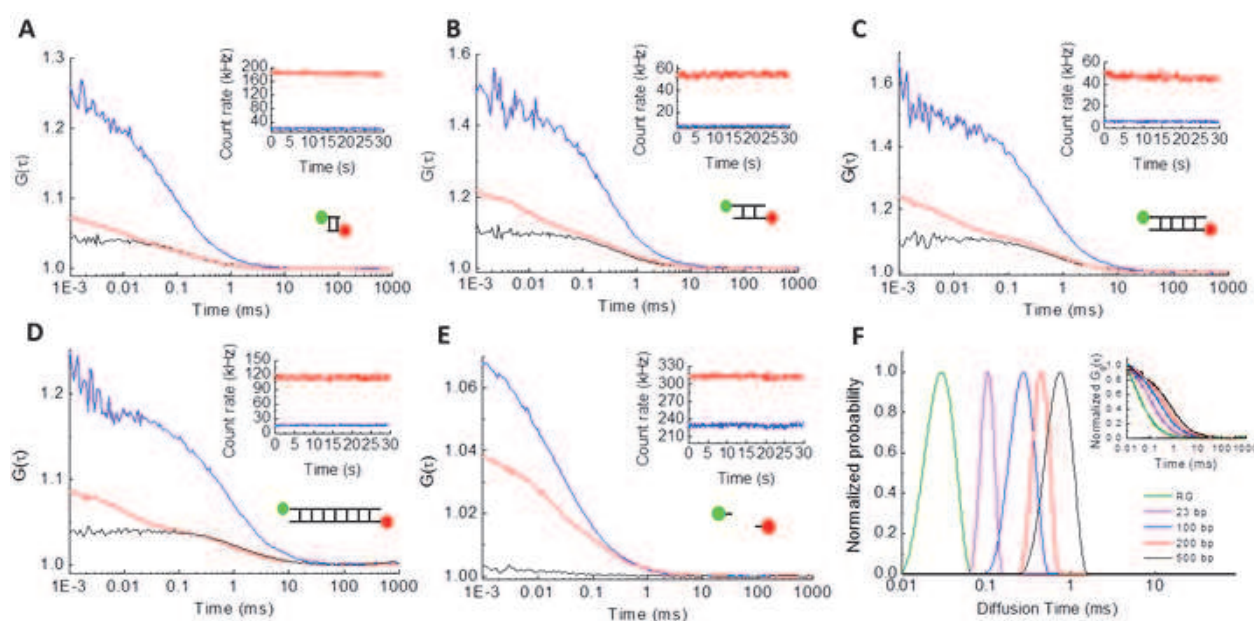


Fig. 5. Characterization of double-fluorescent-labeled DNAs in solution. Auto- and cross-correlation curves of (A) RG-23bp-Cy5 (B) RG-100bp-Cy5 (C) RG-200bp-Cy5 (D) RG-500bp-Cy5 DNA in 10 mM Tris-HCl (pH 7.4). (Insets) The fluorescence intensities in the red (red line) and green (blue line) channels during FCCS measurement. Blue, red and black lines represent $G_g(\tau)$, $G_r(\tau)$ and $G_c(\tau)$, respectively. (E) Auto- and cross-correlation curves of a mixture of RG-primer and Cy5-primer (23 mer each) as a negative control. (F) Distributions of diffusion times $P(\tau D_i)$ of various sizes of RG-DNA-Cy5 calculated from autocorrelation curves of the green channel by CONTIN algorithm. (Inset) Normalized autocorrelation curves $G_g(\tau)/G_g(0)$ (dot) with fitted curves (line) of DNAs in 10 mM Tris-HCl (pH 7.4) at room temperature.

To assess the degree of cross-correlation amplitude, relative cross-correlation amplitude (RCA) was calculated by dividing $G_c(0)-1$ by $G_r(0)-1$. The RCA value was 0.908 ± 0.020 (mean \pm S.D.) for the 500 bp DNA, which had double-fluorescent labels, and 0.104 ± 0.023 for the mixture of fluorescent primers that were used in the PCR reactions (Fig. 5E). The RCA value represents the fraction of DNAs that have RG and Cy5 fluorophores at both DNA ends, thus intact DNAs. To extract information concerning the relative abundance and length of the

DNA from the autocorrelation curve, we used the CONTIN algorithm. The algorithm can determine the distribution of the correlation time with multiple peaks and its probability without any prior assumption about the number of peaks. Figure 5F shows the distributions of diffusion times that were calculated from the autocorrelation curve of the green channel (inset) by using the CONTIN algorithm. The spectra of diffusion times of RG-DNA-Cy5 were separated from each other. This result suggested that the length of the DNA could be estimated with sufficient resolution in this range and length.

3.2 Enzymatic degradation analysis in solution

To confirm whether FCS and FCCS could identify the degradation mechanisms of different kind of nucleases, we monitored the DNA degradation with DNase I (an endonuclease that acts randomly), exonuclease III (an exonuclease that acts in the 3' to 5' direction) and BAL31 nuclease (an exonuclease that acts in both 5' to 3' and 3'to 5' directions) in solution. The nucleases were added to RG-500bp-Cy5 solution in a droplet (50 μ l) on a coverslip and FCCS measurements were performed as a function of time (Fig. 6).

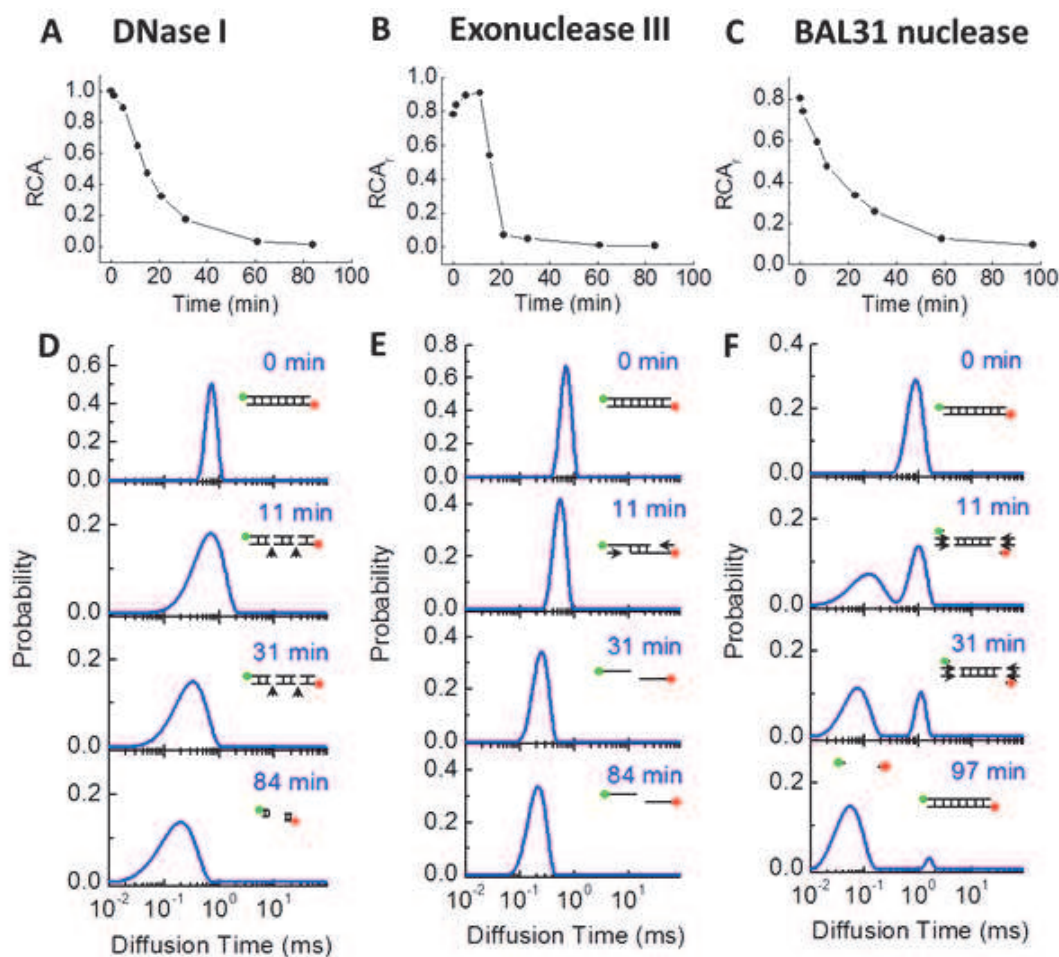


Fig. 6. Relative cross-correlation amplitudes, $(G_c(0)-1)/(G_r(0)-1)$ after addition of (A) 0.0001 U μ l⁻¹ DNase I, (B) 0.02 U μ l⁻¹ exonuclease III, and (C) 0.001 U μ l⁻¹ BAL31 nuclease. Distributions of diffusion times $P(\tau D_i)$ calculated by CONTIN algorithm from $G_g(\tau)$ at several time points after the addition of DNase I (D), exonuclease III (E) and BAL31 nuclease (F).

Figure 6A, B and C show the RCA changes of cross-correlation curves of RG-500bp-Cy5 with the three different type of nucleases. With DNase I and BAL31 nuclease, RCA values rapidly decreased after the nuclease addition. In contrast, with exonuclease III, the RCA value did not decrease until 11 min. This indicated that the fluorophores did not separate in the initial phase of degradation (Fig. 6E insets). The RCA value was not changed without addition of a nuclease in the measurement time (data not shown). We regarded 11 min as the initial phase, 31 min as the transient phase and 84–97 min as the stable phase of enzymatic reaction in Figure 6A, B and C. We performed CONTIN analysis and compared distributions of diffusion times in each phase (Fig. 6D–F). Changing of distribution of diffusion time and RCA show some kind of fingerprint of enzyme activity. The distribution peak became wider and shifted to the left with addition of DNase I (Fig. 6D). The peak width reflects the various lengths of DNA fragments generated by DNase I random degradation. In the case of exonuclease III, the enzyme generates two kinds of single-stranded DNA with the same sizes as the final products. The diffusion time shifted to the left at 31 min after nuclease addition without widening of the peak (Fig. 6E). Interestingly, two distribution peaks were detected with the BAL31 nuclease (Fig. 6F). A faster peak of diffusion times represents small fragments of DNA, with a level of diffusion time comparable to that of the RG fluorophore and a slower peak represents intact DNA. This result is reasonable since the BAL31 nuclease degrades the DNA from both the 5' and 3' ends where the fluorophore is attached. Thus, we could identify the different enzymatic behaviors by using FCCS and distribution analysis of FCS without any separation method such as gel electrophoresis or gel filtration.

3.3 Detection of diffusion properties of exogenous DNAs in cytoplasm

To classify nuclease activity in the cytoplasm of living cells, fluorescent-labeled DNAs were directly introduced into the cytoplasm of living cells by the bead-loading method (Manders et al., 1999, Nagaya et al., 2002). RG-23bp-Cy5 localized largely in the nucleus (Figs. 7A, B, C) though, RG-100bp-Cy5 did not distribute into the nucleus (Figs. 7E, F, G, 8A and C).

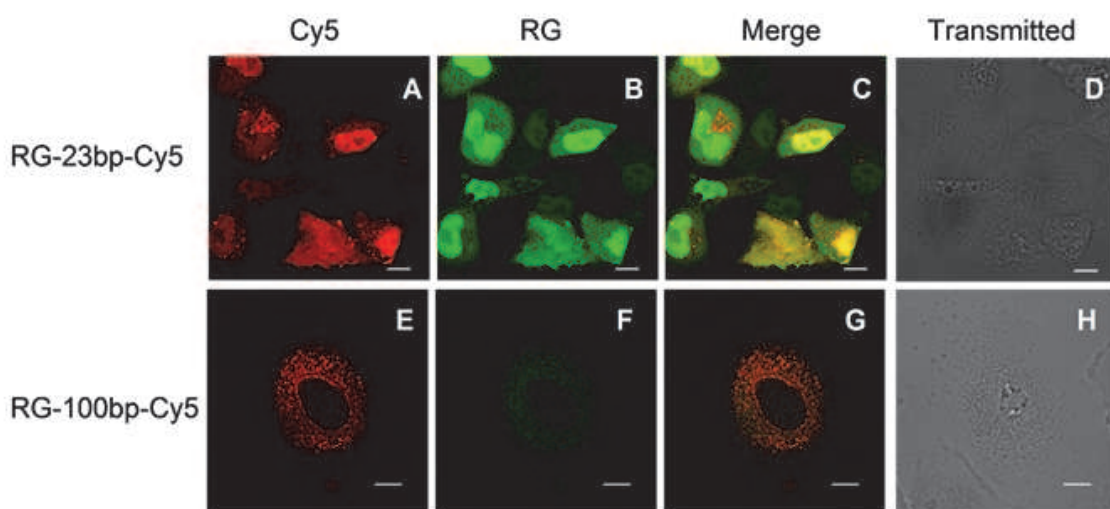


Fig. 7. LSM images of DNA loaded HeLa cells. LSM images of cells 30 min after loading of RG-23bp-Cy5 (A–D) or RG-100bp-Cy5 (E–H). Green (A, E), red (B, F), merged fluorescence images (C, G) and transmitted images (D, H), respectively. Scale bar represents 10 μm .

Auto- and cross-correlation curves of RG-100bp-Cy5 were obtained at the crosshair point in the image of laser scanning microscopy (LSM) of a living cell in which DNAs were incorporated into the cytoplasm (Fig. 8A, C). High cross-correlation amplitude was detected within 10 min after loading (Fig. 8B). However, cross-correlation amplitude was reduced after 45-min incubation at 37°C in the same cell (Fig. 8D). This reduction indicated that exogenous DNA was degraded in cytoplasm. DNA diffusion properties were also analyzed by distributions of diffusion times from autocorrelation curves using the CONTIN algorithm. At 45 min after loading of DNA, a faster peak (around 0.2 ms) appeared in distributions of diffusion times (Fig. 8D inset).

To determine the origin of each peak in the distributions of diffusion times, autocorrelation curves $G_g(\tau)$ s of different DNA sizes that were obtained for the cytoplasm of HeLa cells, and were averaged ($N = 4-8$) and analyzed using the CONTIN algorithm (Fig. 9). Two peaks of diffusion times were detected in each measurement; faster peaks were of the same order of diffusion time as the free RG fluorophore.

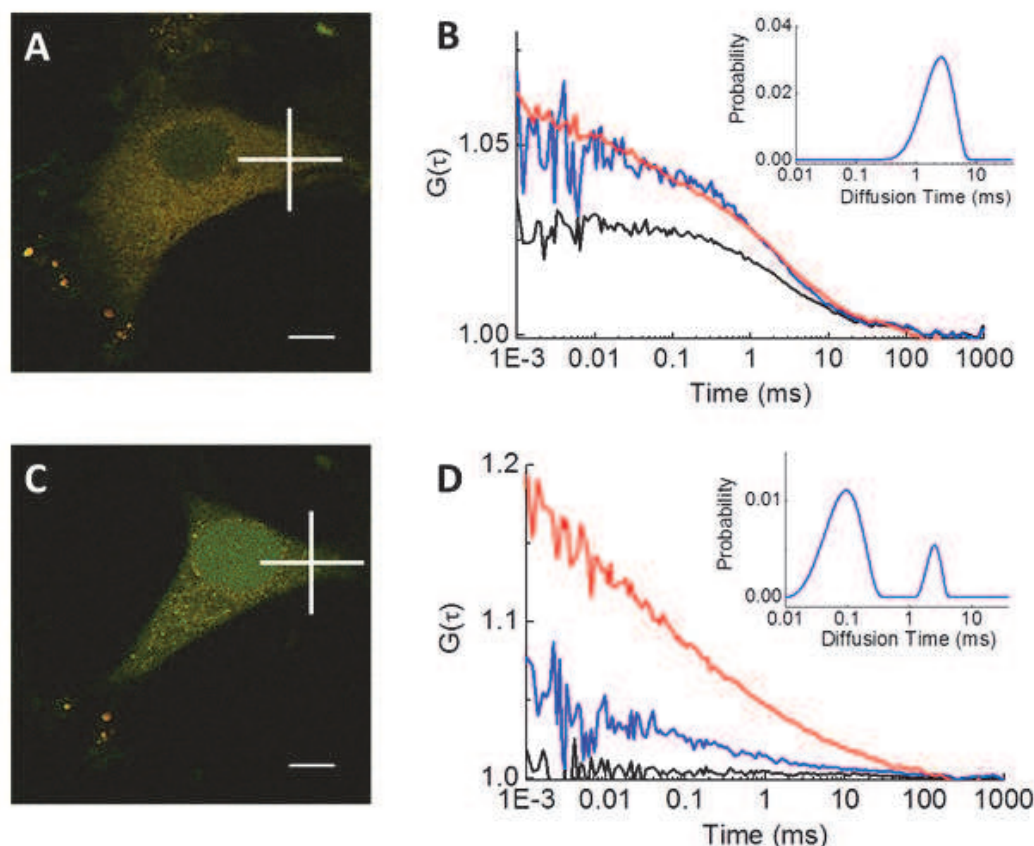


Fig. 8. Nuclease degradation of double-fluorescent-labeled DNAs in cytoplasm of a living COS7 cell. LSM images of (A) 10 min and (C) 45 min after loading of DNAs in the same cell. Auto- and cross-correlation curves of RG-100bp-Cy5 DNA at the crosshairs in the LSM image of (B) panel A (D) panel C. Scale bar represents 10 μm . RG, Cy5 and Cross represent $G_g(\tau)$, $G_r(\tau)$ and $G_c(\tau)$, respectively. Distributions of diffusion times $P(\tau D_i)$ of DNAs calculated by CONTIN algorithm (B, D insets).

On the other hand, the diffusion times of the slower peaks shifted to the right according to the increase in size of incorporated DNA (Fig. 9B). The diffusion times of DNAs in

cytoplasm were 5–10 times slower than those in solution. This ratio was in good agreement with the previously reported value (Dauty et al., 2005) and this result agreed well with the 5' to 3' exonuclease degradation models in solution (Fig. 6F). Finally, the appearance of 5' to 3' exonuclease activity was expected as barrier activity in cytoplasm by comparison of incorporated exogenous DNAs using the distribution pattern of diffusion times. Distribution analysis of diffusion times using CONTIN algorithm clearly showed different peak patterns for different enzymatic activities. The distributions of diffusion times had two peaks in cytoplasm. The diffusion time of the faster peak was almost the same as that of fluorescent dye alone, whereas the other, slower peak depended on the size of the DNA that was incorporated. Moreover, moderately sized DNA fragments were not detected in the cytoplasm. Taken together, these findings helped us to determine that (i) how, (ii) when, and (iii) where incorporated DNAs were degraded in the living cell. (i) The main mechanism of exogenous DNA degradation in cytoplasm was 5' to 3' exonuclease activity rather than endonucleases. (ii) The time scale of degradation (<45 min) was determined by real-time measurement of optical method without invasive treatment. (iii) The location of DNA degradation was not in small compartments but in cytoplasm because the monitored DNAs were distributed homogeneously and had free diffusion values.

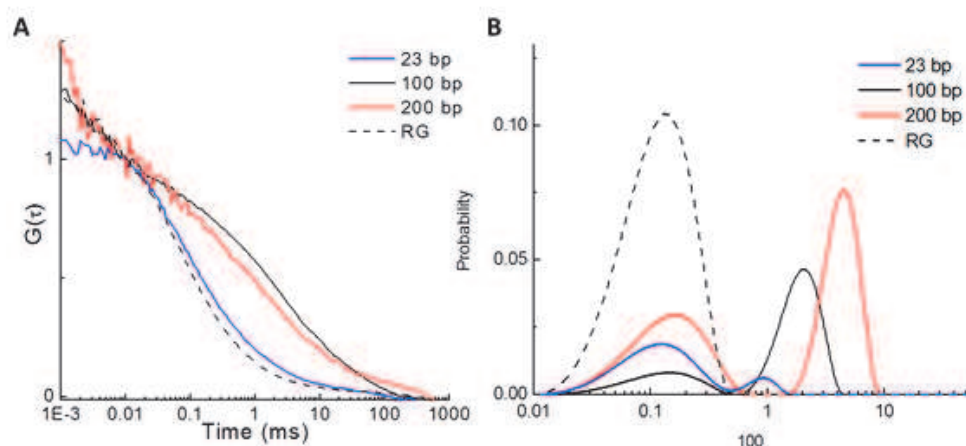


Fig. 9. Relationship between DNA size and diffusion time in living HeLa cells. (A) The average of $G_g(\tau)$ curves in HeLa cytoplasm at 30 min after RG-23bp-Cy5, RG-100bp-Cy5 and RG-200bp-Cy5 loading. (B) Distributions of diffusion times $P(\tau D_i)$ of DNAs calculated from the average of $G_g(\tau)$ curves using CONTIN algorithm. RG dye was also tested as a reference.

3.4 Effect of DNA end-capping on the EGFP expression efficiency

To confirm the enzymatic activity of the 5' to 3' exonuclease in cytoplasm, we carried out an inhibition experiment for the enzyme using end-capped or redundant DNAs and monitoring the expression rate of EGFP. If exonuclease degradation works as a barrier against DNA transfection, the use of longer DNA and/or end-capped-DNA that protects the coding regions from each terminal (Fig. 10) should increase the expression efficiency. We synthesized linear DNAs of various redundancy lengths and capped on both DNA ends by a hairpin-shape oligonucleotide (Zanta et al., 1999, van der Aa et al., 2005). The end-capped DNA remained intact after incubation with exonuclease III (data not shown). Fig. 11 shows

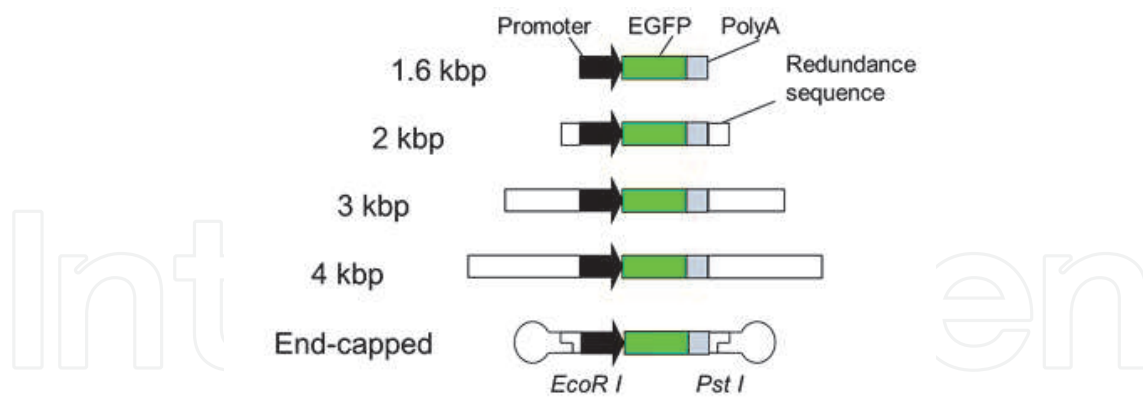


Fig. 10. Schematic diagram of various sizes of DNA expressing EGFP and end-capped DNA.

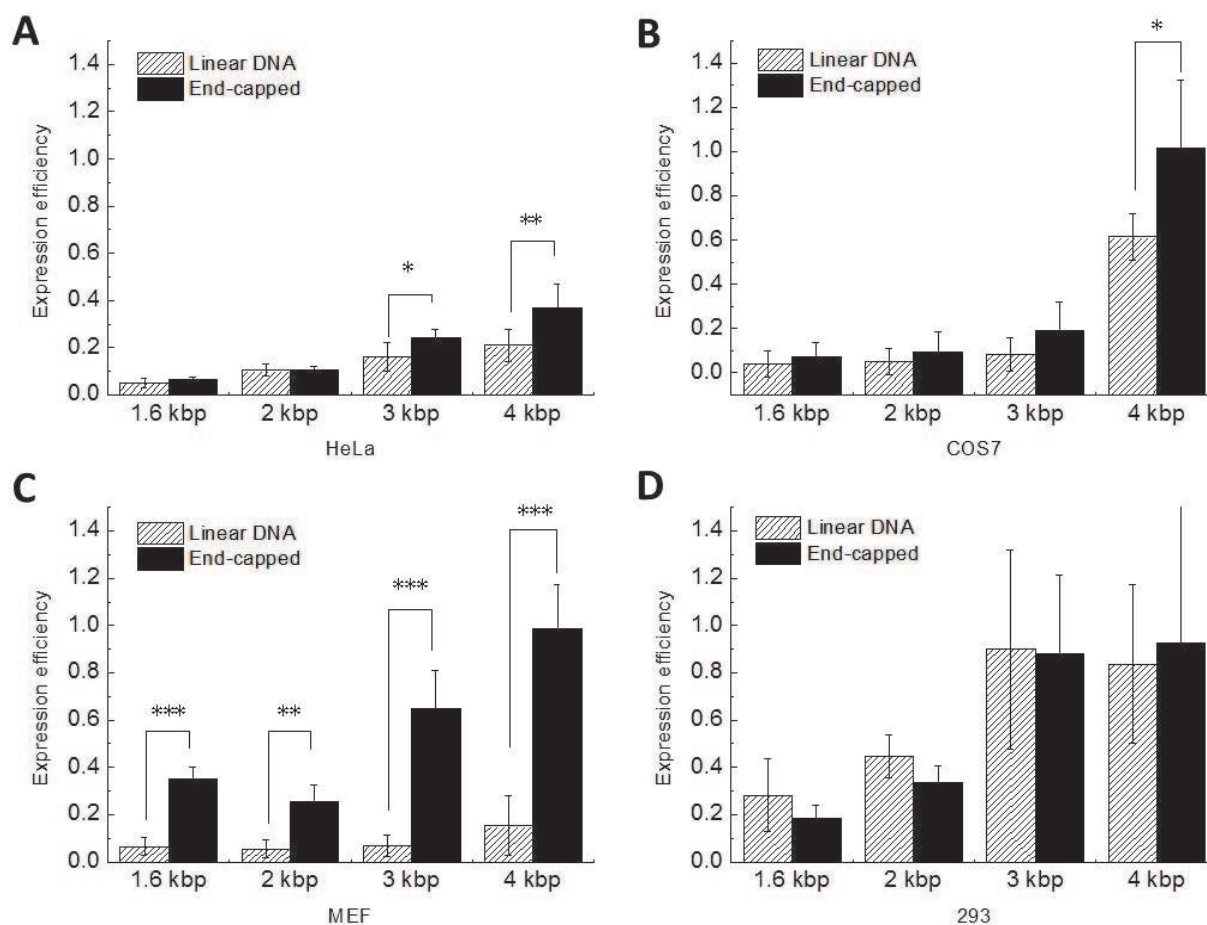


Fig. 11. Effect of DNA protection against exonucleases on expression efficiency with a cationic lipid. (A) HeLa, (B) COS7, (C) MEF and (D) 293 cells were transfected with 1 μ g of uncapped or capped linear DNA per well. Complexes were formed with LipofectAmine 2000 reagent. Expression efficiency (E/Ep) is expressed as the mean \pm S.D. of 4–5 different experiments. To normalize the values from each individual experiment, the expression rate of DNA was divided by the rate using the pEGFP-C1 plasmid. *, $P < 0.05$; **, $P < 0.01$; ***, $P < 0.001$ (Student's t test). Striped bars, uncapped linear DNA; black bars, end-capped DNA.

the expression efficiencies of DNAs in HeLa, COS7, MEF and 293 cells, respectively. The expression efficiency was based on the EGFP expression per copy of transfected DNA ($N \cdot M/W$), the value was divided by the expression of pEGFP-C1 plasmid for normalization ($N_p \cdot M_p/W_p$). The final expression efficiency was calculated by following equation,

$$\text{Expression efficiency} = \frac{N \cdot M/W}{N_p \cdot M_p/W_p} \quad (9)$$

where N , W , and M represent the number of EGFPs obtained from FCS measurement, the transfected DNA weight and molecular weight of transfected DNA, respectively. N_p , W_p and M_p represent the values with the pEGFP-C1 plasmid as a reference.

Expression efficiencies of short DNAs such as that with a 1.6 kbp length were lower than those of other lengths in each cell line. When the expression efficiencies of non-capped PCR products and capped DNAs were compared, it was clear that DNA capping significantly increased the expression efficiency of 4 kbp DNA in HeLa, COS7 and MEF cells. However, the end capping did not enhance the expression rate for short DNA lengths. In MEF cells, uncapped DNAs of all lengths were little expressed and capped DNAs exhibited ~10-fold greater gene expression than the uncapped DNAs. The effect of DNA capping was not observed in 293 cells. Although there were differences in the cell lines, the results obtained for HeLa, COS7 and MEF cells confirmed the effect of exonuclease degradation on DNA transfection. The nuclease activity was inhibited by capped structures on the 3' and 5' ends of the DNA. Interestingly, the end-capping effect on the expression rate was different in the cell lines. In MEF cells, which are generally said to be hard to transfect (Ewert et al., 2006), the end-capping effect was significant (Fig. 11C). On the other hand, in 293 cells, which are generally used in transfection assays because of their high expression efficiency, no end-capping effect was observed (Fig. 11D). These results agreed with previous reports that the transfected plasmids were more stable in 293 cells than in COS, NIH-3T3, HeLa cells (Alwine, 1985). In summary, our results show that exonuclease activity is related to transfection efficiency, though the level of exonuclease activity in cytoplasm might be different depending on the cell line.

Here we propose new concept of nuclease characterization by monitoring the degradation patterns of oligonucleotides based on the fragment size and direction of degradation in living cells. The concept is similar to conventional ones such as an analysis by using radioisotope-labeled oligonucleotides and a size determination by gel electrophoresis. The relationship between the exogenous DNA expression level and DNA stability by extension of DNA fragments was studied using the luciferase assay *in vitro* and *in vivo* (Hirata et al., 2007); however, this assay in a cell homogenate only provides information on bulk DNA stability, not on the individual DNA degradation mechanism. Our approach is, therefore, replacement of the conventional concept by diffusion measurement using a fluorescent tag and coincident analysis using FCS and FCCS so that sensitivity is enhanced to the single molecule level and a physical separation procedure is not needed. Therefore, our method can be employed for measurements in single living cells.

4. Monitoring complex formation between gene carriers and nucleic acids

The association and dissociation between DNA and gene carriers are important *in vitro* and *in vivo*. The efficiency of DNA internalization depends on the properties of DNA/carrier

complexes such as their sizes. The size is determined by affinity between DNAs and carriers and the ratio of DNAs to carrier molecules. The FCCS method has the advantage that it does not need physical separation procedures, so the association and dissociation of DNA and carriers can be directly monitored not only in solution but also in living cells.

4.1 Quantum dot based gene carrier

Quantum dots (QDs) are nanometer-sized semiconductor crystals that emit visible to infrared fluorescence depending on their composition and diameter. QDs have several advantages such as high resistance to photobleaching, high brightness and narrow emission wavelengths with broad excitation spectra. QDs are comprised of an inorganic core, inorganic shell and an organic coating to solubilize them to the water phase. Since the surface to volume ratio of a QD is relatively high, QDs can be used as scaffold particles for carrying ligands, therapeutic agents and gene delivery carriers.

Cationic polymers can condense with DNA by electrostatic interaction to form complexes that promote internalization of exogenous DNA into cells. Polyethyleneimine (PEI) is an efficient gene carrier, that has a proton-sponge effect (Boussif et al., 1995). PEI solubilizes QDs to water so it is also useful for surface coating of QDs (Duan et al., 2007, Zhu et al., 2005).

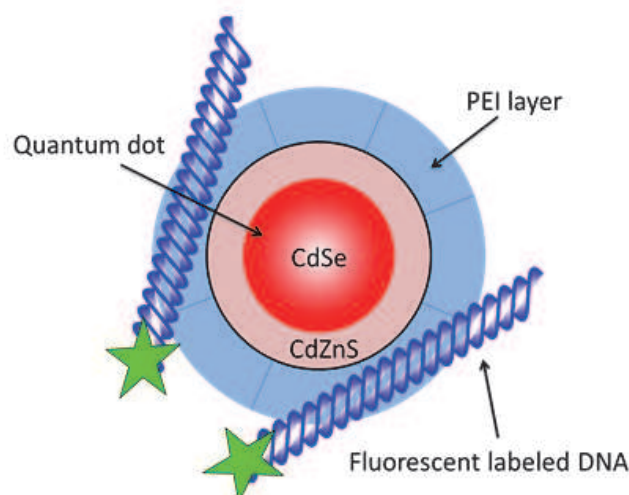


Fig. 12. Diagram of PEI-QD. PEI-coated QD forms a complex with DNA.

CdSe/CdZnS QD cores that emit 605 nm fluorescence were synthesized (Jin et al., 2010) and PEI (average molecular weight about 10000) was added and heated to 60°C in tetrahydrofuran. The resulting precipitates of PEI-coated QDs were dissolved in water (PEI-QDs). The PEI-QD solution was then mixed with a plasmid that coded red fluorescent protein, mKate2 (pmKate2-N). To visualize the localization of the plasmid, a sample plasmid was stained with YOYO-1 iodide. Then the plasmid/PEI-QD complex was added to cultured HeLa cells. After 24-hour incubation, fluorescence emission of expressed mKate2 was detected (Fig. 13). The result showed that PEI-QD had the potential to introduce plasmid vectors into cells. Fluorescence of QDs and YOYO-1 colocalized at large complexes, though free molecules or small complexes were not visible by the conventional microscopy, so methods that can detect their diffusion at the single molecule level, such as FCS and FCCS, are needed.

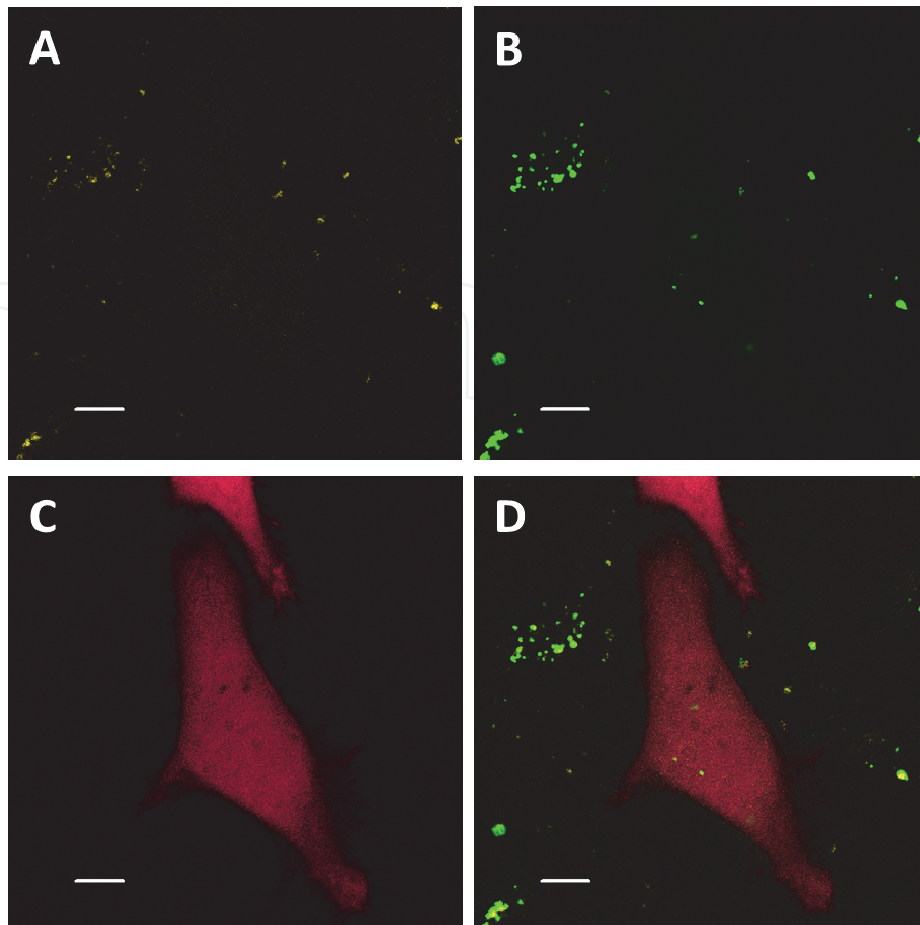


Fig. 13. LSM images of DNA transfected HeLa cells. LSM images of cells 24 hours after addition of PEI-QD/pmKate2-N. QDs (A), YOYO-1 (B), mKate2 (C) and merged fluorescence images (D) respectively. Scale bar represents 10 μm .

4.2 Monitoring of DNA/PEI complex formation in vitro

The efficiency of gene delivery by DNA/carrier complexes depends on the size of the complex and the dissociation kinetics in cells.

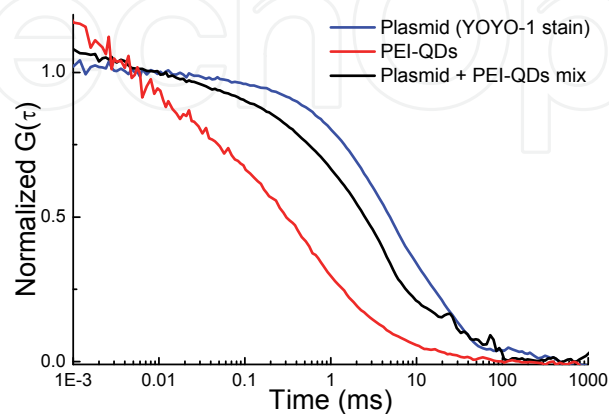


Fig. 14. Normalized autocorrelation curves of plasmid DNA (blue line), PEI-QDs (red line) and a mixture of the plasmid and PEI-QD (black line) in solution.

To develop an efficient gene carrier, it is necessary to characterize the properties of the DNA/carrier complexes. Previously the characterization of complexes was carried out by gel electrophoresis (Eastman et al., 1997).

Currently, there are several FCS studies of DNA/carrier association and dissociation (Van Rompaey et al., 2001, Braeckmans et al., 2010). By using FCS, the size and the ratio of the DNA to the gene carrier are evaluated in solution from the values of the diffusion time and CPM, which are obtained by FCS measurements (see section 2). A 4 kbp circular-shaped plasmid was mixed the PEI-QDs and FCS measurements were carried out. The diffusion time of the plasmid decreased due to the compaction of DNA by the interaction with the cationic gene carrier (Fig. 14).

On the other hand, FCCS can monitor the interaction of DNA with a gene carrier directly. FCS monitors the change of the diffusion time (or molecular size) though the interaction cannot be distinguished if the diffusion time is decreased or not changed due to the change of the molecular shape. For demonstration, PEI-QDs and rhodamine green-labeled 500 bp linear DNA (RG-500bp) were mixed at various ratios, and then FCCS measurements were carried out with single-laser excitation at 488 nm (Fujii et al., 2007). Fluorescence emissions were collected from two channels for rhodamine green and QD. The increase of autocorrelation amplitude of the green channel (RG-500bp) made observation of the DNA complex possible (Fig. 15). The cross-correlation amplitude was also increased (Fig. 15). This high cross-correlation amplitude directly shows the incorporation of RG-500bp and the PEI-QDs.

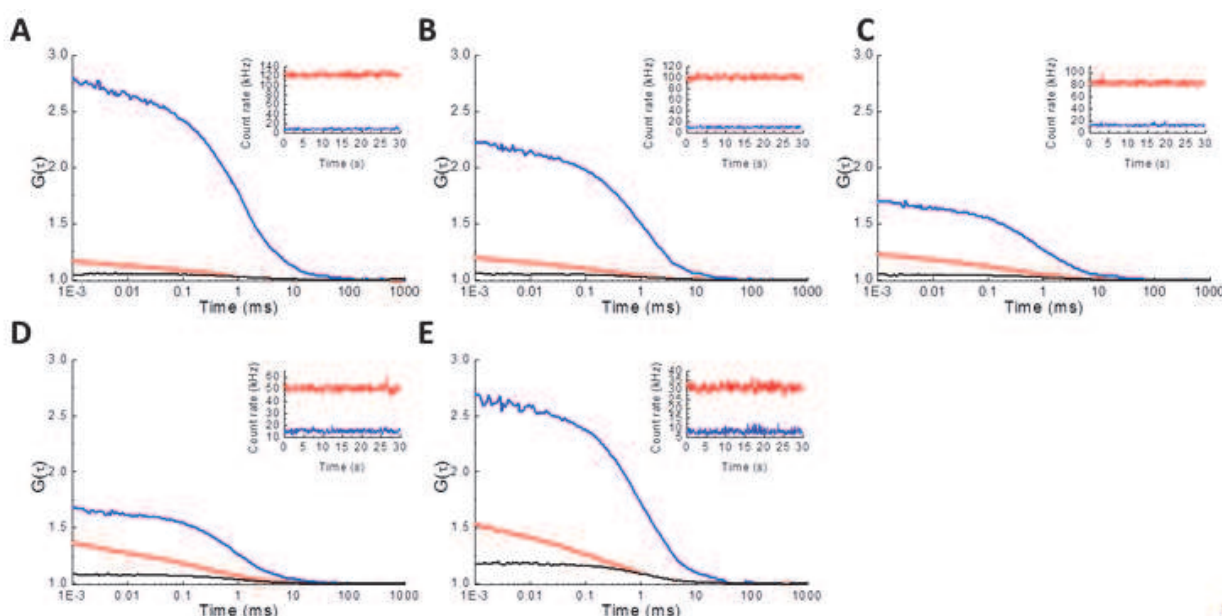


Fig. 15. Cross-correlation analysis of RG-500bp and PEI-QDs. The correlation curves of various RG-500bp/PEI-QD ratios (A; 0.5, B; 1, C; 2, D; 4, E; 8). Blue, red and black lines represent $G_g(\tau)$, $G_r(\tau)$ and $G_c(\tau)$, respectively.

The RCA_r value was increased according to the increase of the PEI-QD concentration (Fig. 16A). At a low DNA/QD ratio, the number of PEI-QDs in solution was larger than the number of RG-500bp so there were many QDs that did not interact with DNA. On the other hand, RCA_g was decreased at once by the decrease of PEI-QD because of the relative decrease of interacting partners (Fig. 16C). The numbers of RG-500bp and PEI-QDs

contained in the complexes could be estimated from the value of CPM. The CPMs of the green channel were 4 to 8 times larger than the value of a single RG-500bp and the CPMs of the red channel were comparable to the value of a single PEI-QD (Fig. 16B). These results indicated that 4 to 8 RG-500bp molecules and a single PEI-QD particle were contained in the complexes under the tested conditions. At high ratios of DNA/QDs, DNA and QDs may aggregate so that RCA_r and CPM_g are increased. The FCCS technique has strong advantages to investigate the properties of DNA carriers such as the strength of binding between DNA and the carrier, the size of the complex and the amount of DNA and number of carriers contained in the complex.

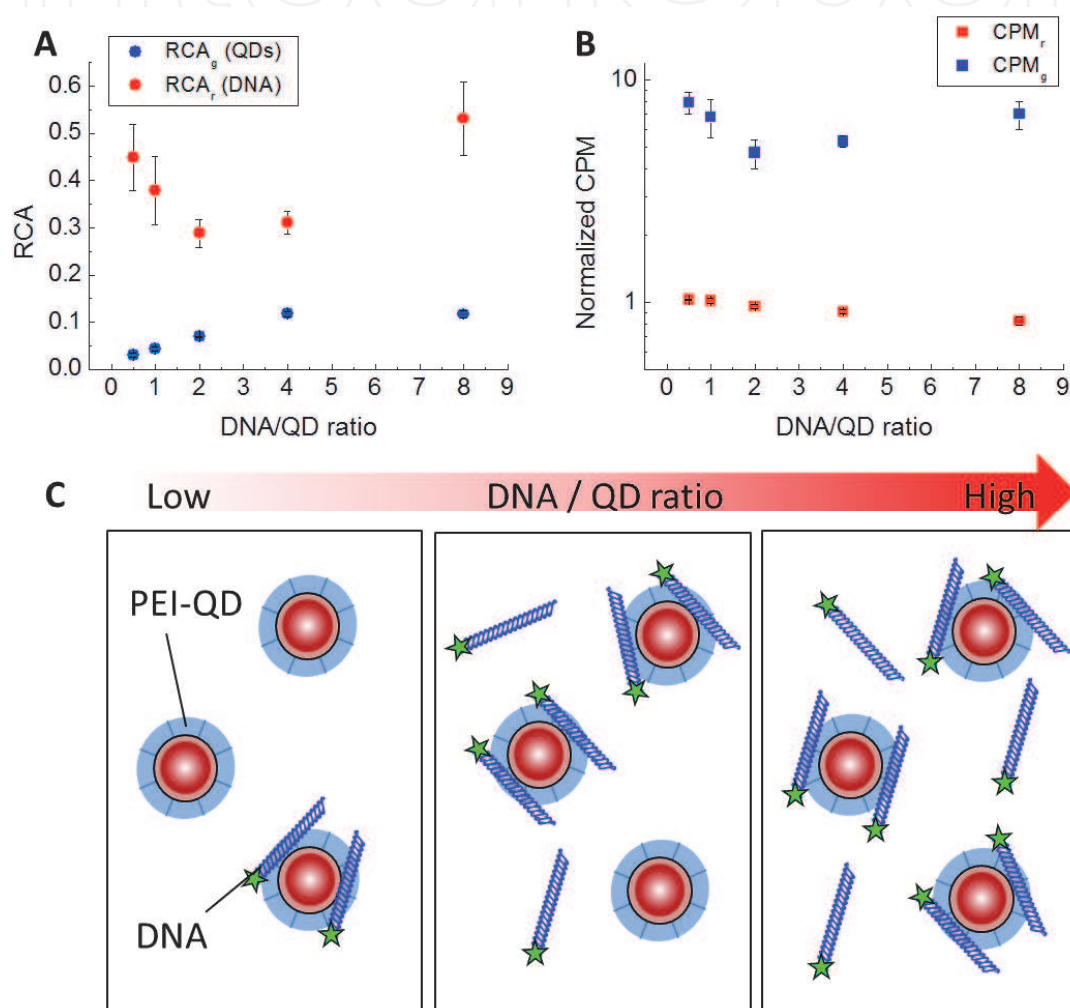


Fig. 16. RCA values (A) and normalized CPM (B) of RG-500bp/PEI-QD complexes. CPM values were normalized by the CPM of a single RG-500bp or PEI-QD. Note that RCA_g shows the ratio of interacting molecules among the red molecules (N_c/N_r). RCA_r shows the ratio of interacting molecules among the green molecules (N_c/N_g) (see Eq. 7 and 8). (C) Schematic diagrams of DNA/QD interactions at various ratios.

5. Conclusion

It is necessary to ascertain the fate of exogenous DNA for the development of nonviral gene therapy. FCS and FCCS, which provide spatiotemporal information on diffusion properties

and interactions of biomolecules, were employed for analyses in living cells. FCCS experiments revealed rapid DNA degradation in cytoplasm. In addition, the DNA degradation mechanism in cytoplasm due to 5' to 3' exonuclease was estimated by measuring DNA diffusion properties at the single molecule level. The methods using noninvasive monitoring of the diffusion properties of DNA provide information on the fate of intracellular exogenous DNA and the efficiency of DNA integration in living cells. Understanding of these intracellular events should help with the development of novel efficient gene delivery methods.

FCS and FCCS are rapidly becoming widely used to detect movements and interactions of biomolecules in living cells (Chenette, 2009, Lidke et al., 2009), and various related applications such as two-focus FCS (Yu et al., 2009), raster image correlation spectroscopy (RICS) (Digman et al., 2009) and multi-point total internal reflection-fluorescence correlation spectroscopy (TIR-FCS) (Ohsugi et al., 2006, 2009) have been developed. FCS, FCCS and these techniques will shed new light on cell biology and gene therapy.

6. Acknowledgements

The authors thank Professor Takashi Jin (Osaka University) for providing various types of quantum dot cores. Our research was partly supported by Grants-in-Aid for Scientific Research (A) 18207010 and (S)21221006, by Grants-in-Aid for Exploratory Research (20657035) from the JSPS, and No. 19058001 in Priority Area "Protein Community."

7. References

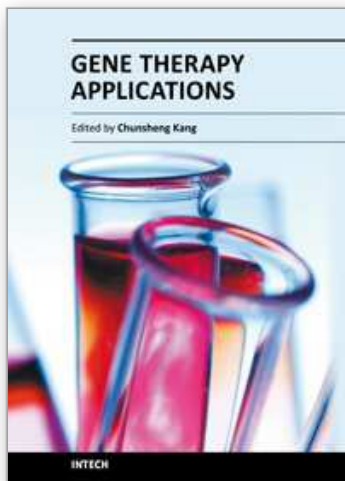
- Alwine, J., (1985). Transient gene expression control: effects of transfected DNA stability and trans-activation by viral early proteins. *Mol Cell Biol*, 5 (5), 1034-42.
- Bacia, K. & Schwille, P., (2007). Practical guidelines for dual-color fluorescence cross-correlation spectroscopy. *Nat Protoc*, 2842-2856.
- Björling, S.; Kinjo, M.; Földes-Papp, Z.; Hagman, E.; Thyberg, P. & Rigler, R., (1998). Fluorescence correlation spectroscopy of enzymatic DNA polymerization. *Biochemistry*, 37 (37), 12971-8.
- Boussif, O.; Lezoualc'h, F.; Zanta, M.; Mergny, M.; Scherman, D.; Demeneix, B. & Behr, J., (1995). A versatile vector for gene and oligonucleotide transfer into cells in culture and in vivo: polyethylenimine. *Proc Natl Acad Sci U S A*, 92 (16), 7297-301.
- Braeckmans, K.; Buyens, K.; Naeye, B.; Vercauteren, D.; Deschout, H.; Raemdonck, K.; Remaut, K.; Sanders, N. N.; Demeester, J. & De Smedt, S. C., (2010). Advanced fluorescence microscopy methods illuminate the transfection pathway of nucleic acid nanoparticles. *J Control Release*, 148 (1), 69-74.
- Chenette, E.J.; (2009). Milestone 10 FCS and FRAP: illuminating cellular processes. *Nat Milestones*, S13-S14
- Chu, G.; Hayakawa, H. & Berg, P., (1987). Electroporation for the efficient transfection of mammalian cells with DNA. *Nucleic Acids Res*, 15 (3), 1311-26.
- Dauty, E. & Verkman, A., (2005). Actin cytoskeleton as the principal determinant of size-dependent DNA mobility in cytoplasm: a new barrier for non-viral gene delivery. *J Biol Chem*, 280 (9), 7823-8.

- Digman, M.; Wiseman, P.; Horwitz, A. & Gratton, E., (2009). Detecting protein complexes in living cells from laser scanning confocal image sequences by the cross correlation raster image spectroscopy method. *Biophys J*, 96 (2), 707-16.
- Duan, H. & Nie, S., (2007). Cell-penetrating quantum dots based on multivalent and endosome-disrupting surface coatings. *J Am Chem Soc*, 129 (11), 3333-8.
- Eastman, S. J.; Siegel, C.; Tousignant, J.; Smith, A. E.; Cheng, S. H. & Scheule, R. K., (1997). Biophysical characterization of cationic lipid: DNA complexes. *Biochim Biophys Acta*, 1325 (1), 41-62.
- Eigen, M. & Rigler, R., (1994). Sorting single molecules: application to diagnostics and evolutionary biotechnology. *Proc Natl Acad Sci U S A*, 91 (13), 5740-7.
- Elouahabi, A. & Ruyschaert, J., (2005). Formation and intracellular trafficking of lipoplexes and polyplexes. *Mol Ther*, 11 (3), 336-47.
- Ewert, K.; Evans, H.; Zidovska, A.; Bouxsein, N.; Ahmad, A. & Safinya, C., (2006). A columnar phase of dendritic lipid-based cationic liposome-DNA complexes for gene delivery: hexagonally ordered cylindrical micelles embedded in a DNA honeycomb lattice. *J Am Chem Soc*, 128 (12), 3998-4006.
- Felgner, P.; Gadek, T.; Holm, M.; Roman, R.; Chan, H.; Wenz, M.; Northrop, J.; Ringold, G. & Danielsen, M., (1987). Lipofection: a highly efficient, lipid-mediated DNA-transfection procedure. *Proc Natl Acad Sci U S A*, 84 (21), 7413-7.
- Fisher, T.; Terhorst, T.; Cao, X. & Wagner, R., (1993). Intracellular disposition and metabolism of fluorescently-labeled unmodified and modified oligonucleotides microinjected into mammalian cells. *Nucleic Acids Res*, 21 (16), 3857-65.
- Fujii, F. & Kinjo, M., (2007). Detection of antigen protein by using fluorescence cross-correlation spectroscopy and quantum-dot-labeled antibodies. *Chembiochem*, 8 (18), 2199-203.
- Hirata, K.; Nishikawa, M.; Kobayashi, N.; Takahashi, Y. & Takakura, Y., (2007). Design of PCR-amplified DNA fragments for in vivo gene delivery: size-dependency on stability and transgene expression. *J Pharm Sci*, 96 (9), 2251-61.
- Jin, T.; Sasaki, A.; Kinjo, M. & Miyazaki, J., (2010). A quantum dot-based ratiometric pH sensor. *Chem Commun (Camb)*, 46 (14), 2408-10.
- Kim, S.; Heinze, K. & Schwille, P., (2007). Fluorescence correlation spectroscopy in living cells. *Nat Methods*, 963-973.
- Kinjo, M.; Sakata, H. & Mikuni, S., (2010). First steps for fluorescence correlation spectroscopy of living cells. *Live Cell Imaging - A Laboratory Manual - second edition*, pp. 229-238, ISBN 978-0-87969-892-8.
- Kinjo, M. & Rigler, R., (1995). Ultrasensitive hybridization analysis using fluorescence correlation spectroscopy. *Nucleic Acids Res*, 23 (10), 1795-9.
- Kitamura, A.; Kubota, H.; Pack, C.; Matsumoto, G.; Hirayama, S.; Takahashi, Y.; Kimura, H.; Kinjo, M.; Morimoto, R. & Nagata, K., (2006). Cytosolic chaperonin prevents polyglutamine toxicity with altering the aggregation state. *Nat Cell Biol*, 8 (10), 1163-70.
- Kogure, T.; Karasawa, S.; Araki, T.; Saito, K.; Kinjo, M. & Miyawaki, A., (2006). A fluorescent variant of a protein from the stony coral *Montipora* facilitates dual-color single-laser fluorescence cross-correlation spectroscopy. *Nat Biotechnol*, 24 (5), 577-81.

- Lechardeur, D.; Sohn, K.; Haardt, M.; Joshi, P.; Monck, M.; Graham, R.; Beatty, B.; Squire, J.; O'Brodivich, H. & Lukacs, G., (1999). Metabolic instability of plasmid DNA in the cytosol: a potential barrier to gene transfer. *Gene Ther*, 6 (4), 482-97.
- Lidke, D. & Wilson, B., (2009). Caught in the act: quantifying protein behaviour in living cells. *Trends Cell Biol*, 19 (11), 566-74.
- Luo, D. & Saltzman, W., (2000). Synthetic DNA delivery systems. *Nat Biotechnol*, 18 (1), 33-7.
- Manders, E.; Kimura, H. & Cook, P., (1999). Direct imaging of DNA in living cells reveals the dynamics of chromosome formation. *J Cell Biol*, 144 (5), 813-21.
- Nagaya, H.; Wada, I.; Jia, Y. & Kanoh, H., (2002). Diacylglycerol kinase delta suppresses ER-to-Golgi traffic via its SAM and PH domains. *Mol Biol Cell*, 13 (1), 302-16.
- Ohsugi, Y.; Saito, K.; Tamura, M. & Kinjo, M., (2006). Lateral mobility of membrane-binding proteins in living cells measured by total internal reflection fluorescence correlation spectroscopy. *Biophys J*, 91 (9), 3456-64.
- Ohsugi, Y. & Kinjo, M., (2009). Multipoint fluorescence correlation spectroscopy with total internal reflection fluorescence microscope. *J Biomed Opt*, 14 (1), 014030.
- Pollard, H.; Toumaniantz, G.; Amos, J.; Avet-Loiseau, H.; Guihard, G.; Behr, J. & Escande, D., (2001). Ca²⁺-sensitive cytosolic nucleases prevent efficient delivery to the nucleus of injected plasmids. *J Gene Med*, 3 (2), 153-64.
- Provencher, S., (1982). A constrained regularization method for inverting data represented by linear algebraic or integral-equations. *Comput Phys Commun*, 27 (3), 213-227.
- Provencher, S., (1982). CONTIN - A general-purpose constrained regularization program for inverting noisy linear algebraic and integral-equations. *Comput Phys Commun*, 27 (3), 229-242.
- Remaut, K.; Lucas, B.; Raemdonck, K.; Braeckmans, K.; Demeester, J. & De Smedt, S., (2007). Can we better understand the intracellular behavior of DNA nanoparticles by fluorescence correlation spectroscopy? *J Control Release*, 121 (1-2), 49-63.
- Rigler, R.; Mets, U.; Widengren, J. & Kask, P., (1993). Fluorescence correlation spectroscopy with high count rate and low-background - analysis of translational diffusion. *Euro Biophys J Biophys Lett*, 169-175.
- Sasaki, A. & Kinjo, M., (2010). Monitoring intracellular degradation of exogenous DNA using diffusion properties. *J Control Release*, 143(1), 104-11.
- Saito, K.; Wada, I.; Tamura, M. & Kinjo, M., (2004). Direct detection of caspase-3 activation in single live cells by cross-correlation analysis. *Biochem Biophys Res Commun*, 324 (2), 849-54.
- Schaffert, D. & Wagner, E., (2008). Gene therapy progress and prospects: synthetic polymer-based systems. *Gene Ther*, 15 (16), 1131-8.
- Selkirk, S., (2004). Gene therapy in clinical medicine. *Postgrad Med J*, 80 (948), 560-70.
- Somiari, S.; Glasspool-Malone, J.; Drabick, J.; Gilbert, R.; Heller, R.; Jaroszeski, M. & Malone, R., (2000). Theory and in vivo application of electroporative gene delivery. *Mol Ther*, 2 (3), 178-87.
- Thomas, C.; Ehrhardt, A. & Kay, M., (2003). Progress and problems with the use of viral vectors for gene therapy. *Nat Rev Genet*, 4 (5), 346-58.
- van der Aa, M.; Koning, G.; van der Gugten, J.; d'Oliveira, C.; Oosting, R.; Hennink, W. & Crommelin, D., (2005). Covalent attachment of an NLS-peptide to linear DNA does not enhance transfection efficiency of cationic polymer based gene delivery systems. *J Control Release*, 101 (1-3), 395-7.

- Van Rompaey, E.; Engelborghs, Y.; Sanders, N.; De Smedt, S. C. & Demeester, J., (2001). Interactions between oligonucleotides and cationic polymers investigated by fluorescence correlation spectroscopy. *Pharm Res*, 18 (7), 928-36.
- Widengren, J.; Mets, U. & Rigler, R., (1995). Fluorescence correlation spectroscopy of triplet-states in solution - a theoretical and experimental-study. *J Physical Chem*, 13368-13379.
- Yu, S.; Burkhardt, M.; Nowak, M.; Ries, J.; Petrásek, Z.; Scholpp, S.; Schwille, P. & Brand, M., (2009). Fgf8 morphogen gradient forms by a source-sink mechanism with freely diffusing molecules. *Nature*, 461 (7263), 533-6.
- Zanta, M.; Belguise-Valladier, P. & Behr, J., (1999). Gene delivery: a single nuclear localization signal peptide is sufficient to carry DNA to the cell nucleus. *Proc Natl Acad Sci U S A*, 96 (1), 91-6.
- Zhang, Y. & Yu, L., (2008). Microinjection as a tool of mechanical delivery. *Curr Opin Biotechnol*, 19 (5), 506-10.
- Zhu, J.; Tang, A.; Law, L. P.; Feng, M.; Ho, K. M.; Lee, D. K.; Harris, F. W. & Li, P., (2005). Amphiphilic core-shell nanoparticles with poly(ethylenimine) shells as potential gene delivery carriers. *Bioconjug Chem*, 16 (1), 139-46.

IntechOpen



Gene Therapy Applications

Edited by Prof. Chunsheng Kang

ISBN 978-953-307-541-9

Hard cover, 492 pages

Publisher InTech

Published online 23, August, 2011

Published in print edition August, 2011

The aim of our book is to provide a detailed discussion of gene therapy application in human diseases. The book brings together major approaches: (1) Gene therapy in blood and vascular system, (2) Gene therapy in orthopedics, (3) Gene therapy in genitourinary system, (4) Gene therapy in other diseases. This source will make clinicians and researchers comfortable with the potential and problems of gene therapy application.

How to reference

In order to correctly reference this scholarly work, feel free to copy and paste the following:

Akira Sasaki and Masataka Kinjo (2011). Fluorescence Cross-Correlation Spectroscopy for Real-Time Monitoring of Exogenous DNA Behavior in Living Cells, Gene Therapy Applications, Prof. Chunsheng Kang (Ed.), ISBN: 978-953-307-541-9, InTech, Available from: <http://www.intechopen.com/books/gene-therapy-applications/fluorescence-cross-correlation-spectroscopy-for-real-time-monitoring-of-exogenous-dna-behavior-in-li>

INTECH
open science | open minds

InTech Europe

University Campus STeP Ri
Slavka Krautzeka 83/A
51000 Rijeka, Croatia
Phone: +385 (51) 770 447
Fax: +385 (51) 686 166
www.intechopen.com

InTech China

Unit 405, Office Block, Hotel Equatorial Shanghai
No.65, Yan An Road (West), Shanghai, 200040, China
中国上海市延安西路65号上海国际贵都大饭店办公楼405单元
Phone: +86-21-62489820
Fax: +86-21-62489821

© 2011 The Author(s). Licensee IntechOpen. This chapter is distributed under the terms of the [Creative Commons Attribution-NonCommercial-ShareAlike-3.0 License](#), which permits use, distribution and reproduction for non-commercial purposes, provided the original is properly cited and derivative works building on this content are distributed under the same license.

IntechOpen

IntechOpen